Effects of Fiber Aggregates on the Transverse Mechanical Behavior of Commingled PP–Glass Fiber Composites

F. Dubouloz-Monnet, N. D. Albérola, P. Mélé

Laboratoire Matériaux Organiques à Propriétés Spécifiques, UMR 5041 CNRS—Université de Savoie, 73376 Le Bourget du Lac Cedex, France

Received 21 October 2004; accepted 12 April 2005
DOI 10.1002/app.22932
Published online 19 January 2006 in Wiley InterScience (www.interscience.wiley.com).

ABSTRACT: In previous articles, mechanical models were proposed to predict the reinforcement effect of polymers by particulates as well as unidirectional fibers over wide ranges of volume fraction of fillers and temperatures. On the basis of image analyses and the definition of representative morphological motifs, these models are able to predict the viscoelastic properties of quasi-isotropic and unidirectional composites or to extract the behavior of a phase, such as the interphase in filled rubbers or the transcrystalline phase in semicrystalline polymers. In this work, based on a 2D image processing, this approach is extended to predict the viscoelastic properties of commingled PP–glass fiber composites. It is shown that fiber aggregates, composed of fibers and surrounding polymer, might be considered as the reinforcing phase. In addition, the different failure modes of these composites are separated as a function of the volume fraction of fillers or temperature. © 2006 Wiley Periodicals, Inc. J Appl Polym Sci 99: 3466–3476, 2006

Key words: composites; homogenization; mechanical properties; morphology; polypropylene

INTRODUCTION

It is well-known that the Achilles' heel of the mechanical behavior of unidirectional glass fiber composites is their response in the transverse (90°) direction.[1] In fact, several researchers have shown that the transverse properties of such materials can be lower than the ultimate properties of unreinforced polymers.[1–4]

The three main origins of this transverse brittleness of unidirectional composites are

i. an insufficient level of adhesion at the fiber–matrix interface, leading to premature debonding,[2]
ii. the dispersion state of fillers within the polymer matrix,[3] and
iii. the triaxial stress state in the polymer matrix.[1,4]

Benzarti et al.[1] have, for example, shown that the improvement of the fiber–matrix adhesion, in a unidirectional glass fibers reinforced epoxy resin, leads to a significant increase in the ultimate properties by using fiber sizing with high epoxy functionality. Asp et al.[4] found that the transverse failure mechanism of composites is governed by the fiber content, the properties of the different phases, and the eventual presence of an interphase. In fact, an increase of the failure stress or strain has been shown when incorporating a soft rubbery interphase between fiber and matrix.[5]

In contrast, Podgaiz and Williams[6] reported a decrease in the transverse failure strain and stress when glass fibers are coated with rubber sizing. The poor performance of such composites has been attributed to the low level of adhesion between the rubbery interphase and the epoxy resin. Vendramini et al.[7] have found that the development of a transcrystalline interphase in commingled PBT–glass fiber composites leads to a significant increase in the transverse shear moduli of composites. An increase in the yield and failure stress has also been observed by these researchers using glass fibers coated with a specific sizing.

By using AFM tapping mode phase imaging and nanoindentation, Gao and Mäder[5] have compared the influence of various fiber sizings on the failure behavior of PP–glass fibers composites. They have shown that the interphase thickness, varying between 100 to 300 nm, depends on the type of sizing. Moreover, they have reported that the formation of a rigid interphase, i.e., with high modulus and a transcrystalline microstructure, leads to an increase in the tensile strength of composites in the longitudinal direction.

For modified PP reinforced by glass fibers coated with various sizings (γ-APS/PU or γ-APS/PP), Mäder et al.[8] have proposed that the dominating mechanism is morphological change in the interphase. These changes are promoted by acid–base interactions, in particular between the basic amino groups at the silanized glass fiber surface and the acid groups of the

Correspondence to: P. Mélé (pmele@univ-savoie.fr).

maleic anhydride grafted matrix. Failure mechanisms of modified PP–glass fiber composites are then related to the properties of the interphase.

Two failure mechanisms have been separated by Gamstedt et al.,[2] a cohesive or an adhesive failure, as a function of the presence or absence of maleic anhydride in PP–glass fiber composites, respectively. The greater fatigue resistance of PP modified with maleic anhydride reinforced by glass fibers has been attributed to the higher interfacial strength between phases and the greater resistance to fiber–matrix debonding.

Accordingly, the quality of adhesion between fiber and matrix plays a major role on the transverse mechanical behavior of unidirectional composites and was analyzed in the present work. The influence of the state of dispersion of unidirectional fibers within the polymer matrix has also been mentioned to explain the transverse brittleness of composites. Different studies have shown that the magnitude of the reinforcement effect depends not only on the physicochemical interactions between phases but also on the filler spatial distribution within the matrix.[9,10]

It is well-known that in modern manufacturing processes, unidirectional thermoplastic composites, fabricated from bundles containing several hundred fibers of polymer and reinforcement, exhibit a heterogeneous spatial distribution of fibers. Vendramini et al.[7] and Dubouloz-Monnet et al.[11] have shown that fibers are packed into clusters in commingled composites. On the basis of percolation concept, Alberola et al.[9] have developed a micromechanical model to separate the relative contributions of clusters to changes in the microstructure of polymer induced by glass fibers.

In this work, we first propose to give evidence of the influence of fiber aggregates on the viscoelastic properties of commingled composites and then to correlate the spatial distribution of fibers to the macroscopic failure behavior of such composite materials.

EXPERIMENTAL

Raw materials

Two polymers were used in this study. The first, an unmodified polypropylene supplied by the Montell Polyolefins Company, has a weight average molecular mass, M_w, equal to 263400 g/mol and an index of polydispersity equal to 5.6. The second one is a maleic anhydride grafted polypropylene provided by the Uniroyal Chemical Company.

The filaments of polypropylene, processed by the Vetrotex International Company, are obtained from a main mixture consisting of 80% of chemically unmodified matrix and 20% of maleic anhydride grafted matrix. They are processed by extrusion at 200°C, and then hot drawn at a constant rate.

Unidirectional glass fibers, supplied by the Vetrotex, have a monodisperse distribution diameter of about 17.5 μm,[11] and coated with a specific sizing for the polypropylene matrix.

TABLE I
Weight (W_f), Volume (V_f), and Surface (S_f) Contents of Glass Fibers

Composite	W_f (%)[a]	V_f (%)[b]	S_f (%)[c]
T22	44.3 ± 0.2	21.6 ± 0.2	21.8 ± 1.7
T35	61.5 ± 0.2	35.6 ± 0.2	34.9 ± 2.6
T50	74.3 ± 0.1	50.0 ± 0.1	49.9 ± 2.1

[a] Determined from residues of burned samples at 625°C.
[b] Derived from weight content.
[c] Evaluated by image analysis.

Sample preparation

Glass fibers are directly commingled with polymer filaments during the manufacture of the roving. The sheets of unidirectional commingled composites, processed by Vetrotex under the trade name of Twintex®, are carried out by filament winding of polymer and glass roving. These mixed fibers are hot consolidated under pressure. Unidirectional fiber composites are then cured for the same conditions as those used for the unfilled materials, to give the same thermal history for each sample.

In this work, composites reinforced by three different amounts of glass fibers were studied. The weight contents of fillers, the volume fractions, and the corresponding surface ratios as well as the nomenclature used are presented in Table I.

A previous study has shown that the porosity or the void content, evaluated by image analysis, can be considered negligible in the different composites.[12]

Test procedures

Dynamic tensile mechanical spectrometry is performed in a transverse mode on unreinforced polymer and composite materials by using a VA 4000 apparatus commercialized by the 01 dB Metravib Company. The real (E'_T) and imaginary (E'_T) parts of the complex transverse Young's modulus, E^*_T, and the damping ratio, tan δ_{ET}, are determined as a function of temperature and/or frequency.

Two kinds of tests are carried out:

i. Isochronal spectra at 1 Hz are recorded for temperatures ranging from −70 to 125°C with a heating rate of about 1°C/min. The dynamic strain imposed to the different samples was about 0.075%, to remain in the linear domain, whatever the temperature analyzed.
ii. The influence of the dynamic strain, from 0.005 to 150%, on the transverse mechanical behavior of the unfilled material and commingled com-

posites was also analyzed at 1 Hz for various temperatures (−90, −50, −10, 30, and 70°C).

Microindentation measurements are carried out with a Leco M400 H3 microhardness tester. The different tests are performed by using a Knoop indenter and a load of 0.05 N. The lengths of both imprints are measured within 10 s following indentation. The microhardness values (H_K) are then calculated by using the following expression:[13,14]

$$H_K = 14.23 \frac{P}{d^2} 10^{-6} \quad (1)$$

where *HK* is expressed in megapascals, the applied force *P* in newtons and the imprint length *d* in meters. Ten measurements are made on each material at a constant distance of 15 μm from the surface of the glass fibers to limit the influence of the different polishing steps occurring during the sample preparation. Moreover, additional measurements are performed at different distances from the fiber surface to show an eventual gradient of microhardness as a function of the fiber surface.

The fracture surfaces of unidirectional composites are then observed with a scanning electron microscope (model Stereoscan 440, Leica) in secondary electron detection mode. All surfaces are previously coated with gold to avoid charging under the electron beam.

RESULTS AND DISCUSSION

Experimental viscoelastic behavior

Figure 1 shows the experimental variations of (a) E'_T, (b) E''_T, and (c) tan δ_{ET} as a function of the temperature for unfilled polymer and the T22, T35, and T50 composites at 1 Hz. The increase in the real and the imaginary parts of the transverse Young's modulus over the temperature range analyzed, accompanied by the decrease in the maximum damping factor for temperatures lower than 25°C, can be attributed not only to the usual reinforcement effect induced by glass fibers but also to an enhancement of this effect due to the presence of fiber aggregates.[7,9]

It can also be observed, for temperatures greater than 25°C, that the damping factor of the different composites is insensitive to the filler content. The origin of such a relaxation, so-called α', remains controversial. In fact, in the literature, this relaxation has been associated to either the presence of defects in the crystalline phase or mechanisms implying both the amorphous and crystalline phases.[15–18]

Consequently, modifications of the viscoelasticity of commingled composites can originate from the mechanical coupling effect enhanced by (i) the formation of aggregates or (ii) the microstructural changes of the polypropylene matrix. In fact, Dubouloz-Monnet et al.[12] have shown that glass fibers act as nucleating agents for the polypropylene matrix. To separate their relative contributions on the transverse mechanical behavior of composites, a micromechanical model is proposed in this article, based on a morphological analysis.

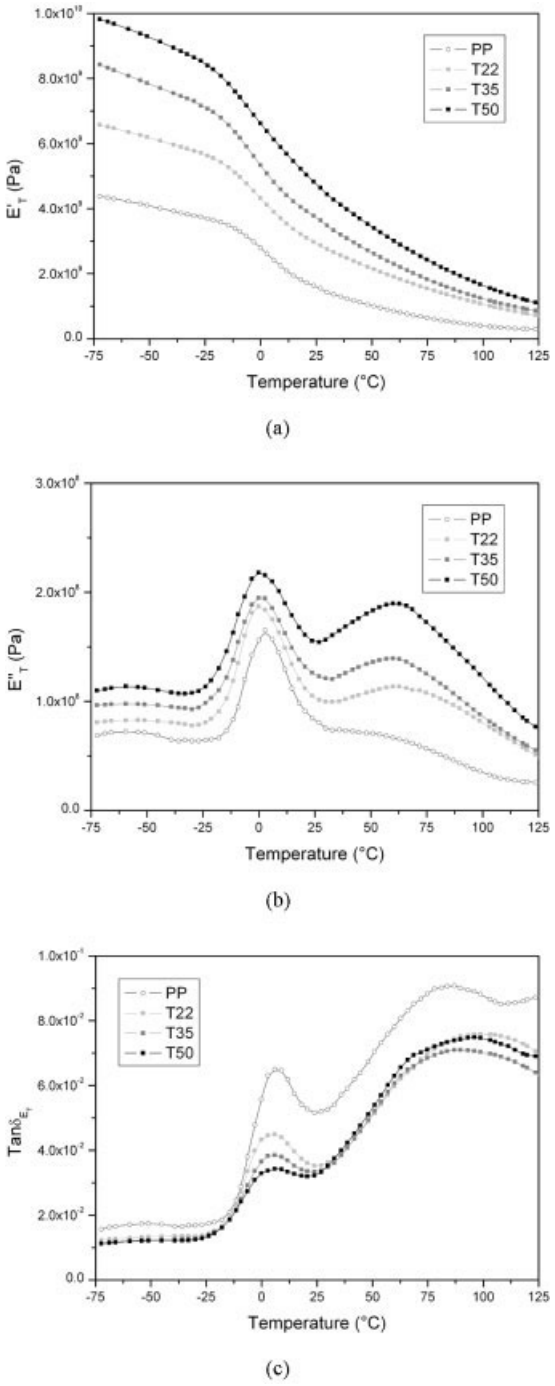

Figure 1 Experimental variations of (a) E'_T, (b) E''_T, and (c) tan δ_{ET} *versus* temperature at 1 Hz for T22, T35, and T50 composites. Data for unreinforced polymer are also reported for comparison.

TABLE II
Values of Morphological Parameters of Commingled Composites Studied[a]

Composite	S_f (%)	S_{ag} (%)	χ_0
T22	21.8 ± 1.7	26.0 ± 3.0	0.18 ± 0.02
T35	34.9 ± 2.6	42.6 ± 4.6	0.20 ± 0.03
T50	49.9 ± 2.1	59.9 ± 3.3	0.20 ± 0.03

[a] Extracted from ref. 19.

Modeling of the reinforcement effect

Using a 2D image processing, Dubouloz-Monnet et al.[19] have shown that the composites exhibit a heterogeneous morphology characterized by both isolated fibers and aggregates. In fact, more than 86% of glass fibers are packed into aggregates randomly dispersed within the polymer matrix. Two reinforcing phases can be then considered:

i. glass fibers, at a microscopic scale and
ii. fiber aggregates, at a mesoscopic scale.

Moreover, different geometric characteristics of such clusters have been determined, such as the surface fractions of fibers and aggregates, S_f and S_{ag}, and a morphological parameter, χ_0, defined by the following relationship[9,19] (Table II):

$$X_0 = \frac{S_{ag} - S_f}{S_f} \tag{2}$$

To define the phase considered as the reinforcing one, micromechanical modeling is performed. Benzarti[20] and Vendramini et al.[7] have shown that if glass fiber is assumed as the reinforcing phase, embedded in the polymer, important differences can be observed between theoretical and experimental values. The same conclusion has been made when we assumed glass fibers well dispersed within the polypropylene matrix acting as the reinforcing phase.[11] In fact, theoretical data tends to underestimate experimental ones in the whole temperature range.

The first objective of this work was to consider fiber aggregates as the reinforcing phase. The problem is to assign values for their properties. The prediction of the viscoelastic behavior of commingled composites can then be assessed by assuming the aggregates as the reinforcing phase.

Prediction of the viscoelastic properties of fiber aggregates

To account for the presence of clusters, we defined the following "representative morphological pattern" (RMP), whatever the glass fiber content. This RMP consists of a two-layered cylindrical inclusion, in which phase 1 is the glass fiber surrounded by a shell of polymer (phase 2), embedded in the equivalent homogeneous medium (Fig. 2). The elastic properties of aggregates can be predicted by using a (3)-phase self-consistent scheme derived from the models developed by both Hashin and Rosen[21] and Christensen and Lo[22,23] and extended to the viscoelastic behavior by applying the correspondence principle.[24]

The complex transverse Young's modulus of aggregates, E^*_{Tag}, can be expressed by the following relationship:

$$E^*_{Tag} = \frac{2}{\dfrac{1}{2K^*_{Tag}} + \dfrac{1}{2G^*_{TTag}} + \dfrac{2\nu^{*2}_{LTag}}{E^*_{Lag}}} \tag{3}$$

where G^*_{TTag} and K^*_{Tag} are the complex transverse shear and the plane-strain bulk moduli of the aggregates, respectively. E^*_{Tag} and ν^*_{Tag} are the complex longitudinal Young's modulus and Poisson's ratio of the aggregates, respectively.

Moreover, for numerical simulations, it is assumed that

i. glass fibers show an elastic behavior over the analyzed temperature range. Young's modulus and Poisson's ratio of fibers are assumed to be constant and equal to 73 GPa and 0.22, respectively;
ii. viscoelastic properties of the matrix are assumed to be the same as those of the unreinforced polymer, to give evidence for the influence of the geometric arrangement of fibers;
iii. to account for the glass–rubber transition undergone by the polymer through the glass transition, the real part of the Poisson's ratio of the matrix is assumed to vary from 0.30 to about 0.40 for temperatures higher than that of the glass transition.[25]

Values of the surface fractions of fibers and aggregates are derived from a previous morphological analysis. The theoretical behavior of the transverse Young's modulus of aggregates *versus* temperature is depicted in Figure 3. The viscoelastic properties of the unfilled polymer and T50 composite are superimposed for comparison. It can be seen that the viscoelastic properties of fiber aggregates are significantly greater than

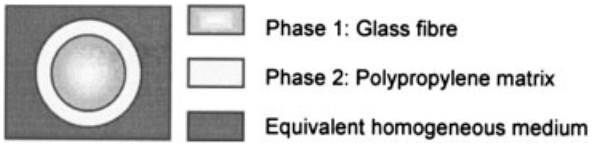

Figure 2 Definition of the RMP.

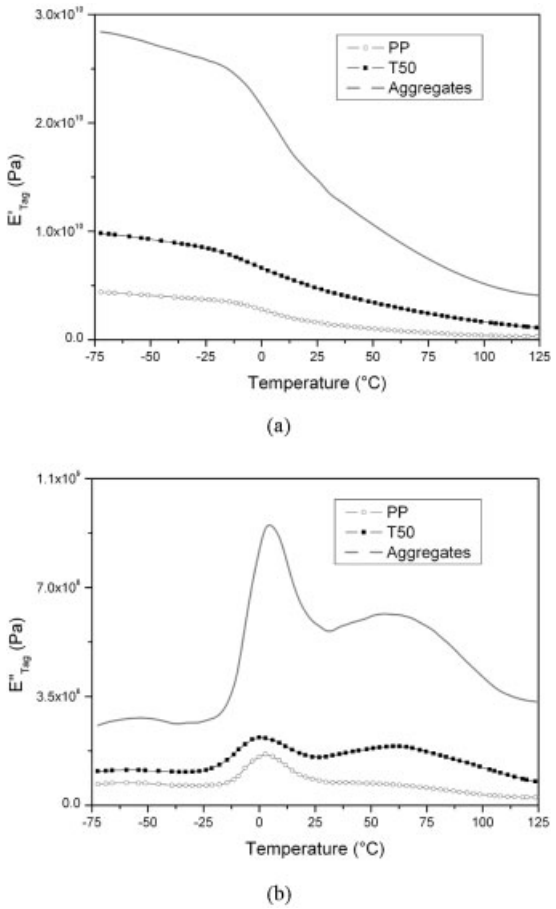

Figure 3 Theoretical variations of (a) E'_{Tag} and (b) E''_{Tag} for the aggregates as function of the temperature. Experimental results are also reported for the unfilled polymer and the T50 composite.

those of the highest filled material over the temperature range analyzed.

The values of the other glassy elastic properties for the aggregates, i.e., the complex transverse shear (G^*_{Tag}), the plane-strain bulk (K^*_{Tag}), the longitudinal Young's moduli (E^*_{Tag}), and the Poisson's ratio (ν^*_{Tag}), are listed in Table III for the glassy domain. It has been shown that the glassy transverse Young's modulus of aggregates, $E^*_{Tag,}$ depends not on the filler content but on the value of the χ_0 parameter corresponding to the relative amount of polymer within the aggregates. The longitudinal Young's modulus of aggregates ranges from 60 to 65 GPa for the different composites analyzed in the glassy state.

TABLE III
Values of the Real Parts of the Complex Transverse Shear (G'_{TTag}), Plane-strain Bulk (K'_{Tag}), and Longitudinal Young's Moduli (E'_{Lag}) of the Aggregates Evaluated for a χ_0 Value Equal to 0.19 at −50°C

G'_{TTag} (GPa)	E'_{Tag} (GPa)	K'_{Tag} (GPa)	E'_{Lag} (GPa)	ν'_{LTag}[a]
13.1	33.4	25.0	64.7	0.23

[a] Poisson's Ratio.

TABLE IV
Values of 2D Geometrical Parameters of Aggregates[a]

Composite	R_{ag} (μm)	Δ_{ag} (μm)	R_s (μm)
T22	31 ± 2	63 ± 4	62 ± 4
T35	37 ± 3	36 ± 4	55 ± 4
T50	30 ± 2	18 ± 3	39 ± 3

[a] Extracted from ref. 19.

Prediction of the viscoelastic properties of composites

On the basis of viscoelastic properties of aggregates, the prediction of the mechanical behavior of unidirectional composites can now be determined. A previous morphological analysis has shown that fiber aggregates are randomly dispersed within the polymer matrix, whatever the content of fillers.[19]

Moreover, this analysis enables us to determine several geometrical parameters, such as their radius, R_{ag}, the interaggregate surface-to-surface distance, Δ_{ag}, and the radius of the polymer shell surrounding the aggregates, R_s, characteristic of aggregates, from the analysis of the autocorrelation function and Fast-Fourier Transform (FFT) power spectrum [Table IV and Fig. 4(a)].

The second RMP chosen is then composed of the fiber aggregate (phase 1) surrounded by a shell of polymer (phase 2). The transverse Young's modulus of composites, $E^*_{Tc,}$ can be determined through the following expression:

$$E^*_{Tc} = \frac{2}{\frac{1}{2K^*_{Tc}} + \frac{1}{2G^*_{TTc}} + \frac{2\nu^{*2}_{LTc}}{E^*_{Lc}}} \quad (4)$$

where G^*_{TTag} and K^*_{Tag} are the complex transverse shear and the plane-strain bulk moduli of the composites, respectively. E^*_{Lc} and ν^*_{LTc} are the complex longitudinal Young's modulus and Poisson's ratio of the composites, respectively. Detailed calculations of such parameters are given in the APPENDIX. According to Hashin,[26,27] these expressions developed for isotropic elastic phases remain valid for the phases which are themselves transversely isotropic.

The comparison between experimental and theoretical transverse Young's moduli of composites for the T22, T35, and T50 materials are depicted in Figure 5. A good agreement between experimental and predicted values can be noted in the glassy domain for all the composites studied. This result shows that the fiber aggregates act as the reinforcing phase, and the microstructural changes in the polypropylene matrix do

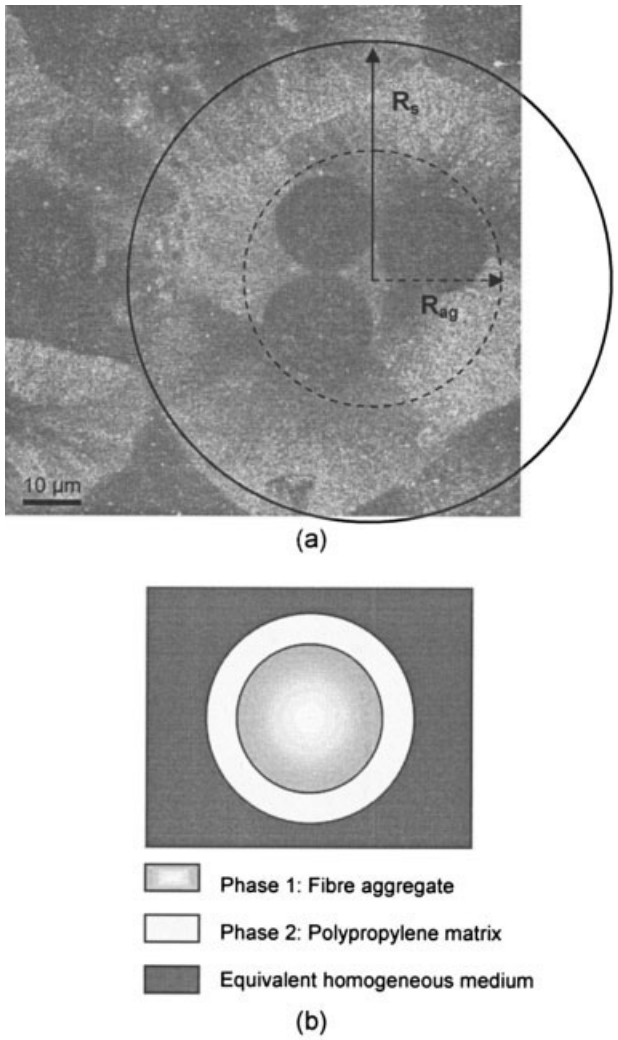

Figure 4 (a) Optical observation of the T22 composite and (b) definition of the corresponding RMP.

not affect the macroscopic properties of commingled composites in this temperature range.

In contrast, for temperatures greater than about 0°C, the model tends to underestimate the rubbery modulus of composites, whatever the fraction of fillers. These differences can originate from modifications of the microstructure of polymer induced by the presence of glass fibers.[12]

Unlike PBT–glass fiber composites, it has been shown that no difference exists in birefringence between the polymer matrix in the bulk and close to the fiber surface.[7,12] Moreover, no difference was detected between the degree of crystallinity of polymer matrix and that of the unreinforced polypropylene. The only difference revealed between the thermograms of PP–glass fiber composites compared with those of the unfilled polymer is that the polymer reinforced by unidirectional fibers has a lower melting temperature related to a global modification of the crystalline organization.[12]

To show the influence of these microstructural changes on the macroscopic mechanical behavior of the composites, microindentation tests are then performed at 25°C [Fig. 6(a)]. Microindentation tests have been previously used to assess the interfacial properties in polymer–glass fiber systems.[28] Analytical models have also been proposed by several researchers to evaluate the interfacial shear strength of glass-reinforced composites.[29,30]

Mean values of microhardness H_K of unfilled PP and commingled composites are shown in Figure 6(b). It can be observed that

i. the mean microhardness values for the polymer matrix are greater than that of the unfilled polymer, whatever the volume fraction of fibers;
ii. the average H_K values of polymer matrix decrease with increase in volume fraction of fillers; and
iii. no significant difference in the H_K values of polymer matrix has been noted as a function of the distance from the glass fiber surface, charac-

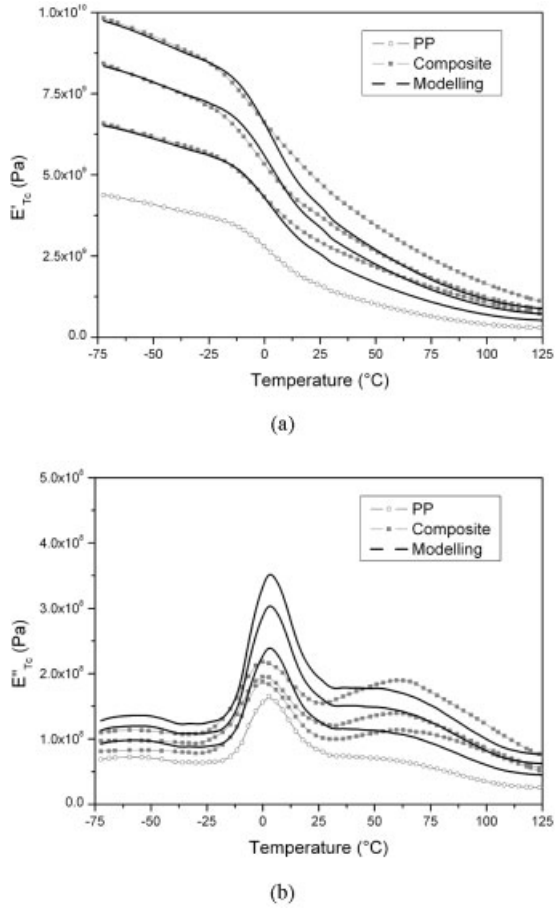

Figure 5 Comparison between theoretical and experimental values of (a) E'_{Tc} and (b) E''_{Tc} as a function of the temperature for the different composites.

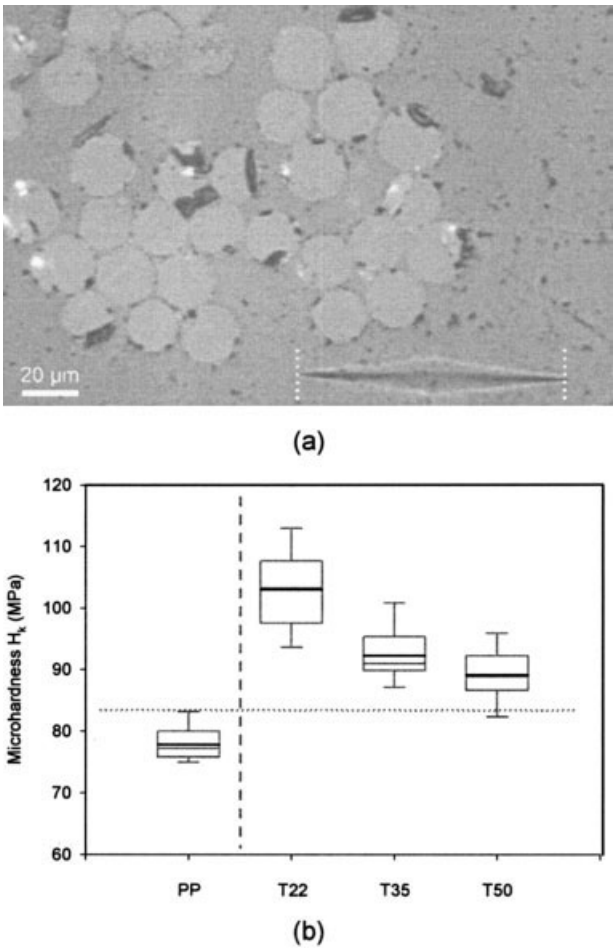

Figure 6 Microindentation tests: (a) imprint in the T22 composite and (b) experimental values of H_K for the different materials.

teristic of the formation of a broad interphase.[10,11]

Accordingly, these results confirm the global changes of the crystalline organization of the polypropylene matrix induced by glass fibers, which are in agreement with previous DSC analysis.[12] The modifications in the crystallite size, which act as physical ties, affect the molecular mobility of the amorphous phase of the polypropylene matrix, in particular at temperatures higher than T_g. This result can explain the greater values of the experimental transverse Young's modulus of the different composites compared with theoretical ones in the rubbery region.

Experimental mechanical behavior at large strains

The last part of this article concerns the influence of fiber aggregates on the transverse mechanical behavior of commingled composites. The eventual correlation between morphological parameters and critical values of deformation might help us to define the origins of the transverse brittleness of PP–glass fiber commingled composites.

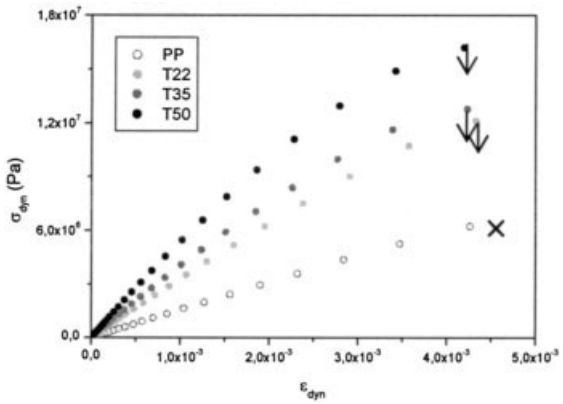

Figure 7 Experimental variations of σ_{dyn} as a function of ε_{dyn} at 30°C and 1 Hz for the materials studied.

The behavior of the dynamic stress, σ_{dyn}, *versus* the strain amplitude, ε_{dyn}, at 30°C and 1 Hz for the different materials are depicted in Figure 7 (arrows correspond to the mean values of failure strain of composite materials, whereas the cross marks the characteristic yield strain of unfilled polypropylene). From these stress–strain curves, it can be observed that the dynamic stress is strongly dependent on the fiber content. In fact, with increase in volume content of fillers, a significant increase in the failure stress can be observed, characteristic of a good load transfer at the fiber–polymer interface. A small decrease in the transverse Young's modulus with the amplitude of deformation can also be shown, corresponding to damage initiation.[31]

To determine precisely the value of this critical deformation, defined as ε_c, the behavior of the damping factor, tan δ_{ET}, as a function of the strain amplitude is plotted in Figure 8.

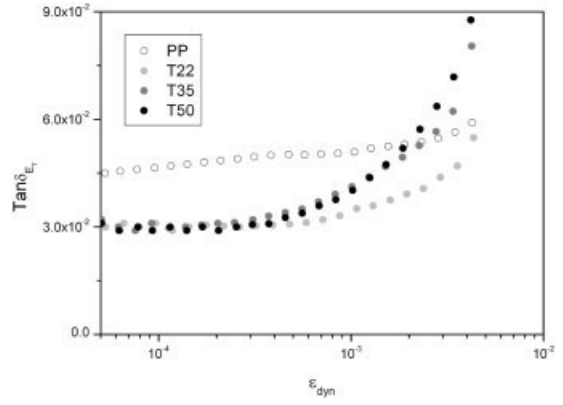

Figure 8 Experimental variations of tan δ_{ET} *versus* the dynamic strain ε_{dyn} for the different materials at 1 Hz and 30°C.

TABLE V
Values of the Critical Strain (ε_c) for the Different Composites Determined at 30°C and 1 Hz

Composite	ε_c ($\times 10^4$)
T22	3.6 ± 0.4
T35	2.5 ± 0.1
T50	1.7 ± 0.1

The decrease in the transverse Young's modulus of composites can in fact be related to the increase in the dissipative part of E^*_T. An important decrease in the values of ε_c with an increase in filler content can be seen (Table V), related to additional dissipative phenomena induced by the damage of

i. the fiber–polymer interface,
ii. the aggregate–polymer interface, and
iii. the matrix polymer.

The differentiation between these different local mechanisms are discussed in the next section.

Influences of filler content and temperature on the damage of composites

The evolution of the critical deformation, ε_c, *versus* the temperature for the different materials is depicted in Figure 9. Two domains can be distinguished, corresponding to the glassy and rubbery regions of the polymer matrix:

i. for temperatures lower or equal to −10°C, values of ε_c for the different materials remain constant. ε_c is only dependent on the filler content.
ii. for temperatures greater than −10°C, ε_c slightly increases for the unfilled polymer, whereas it first decreases and then remains constant for all the composites.

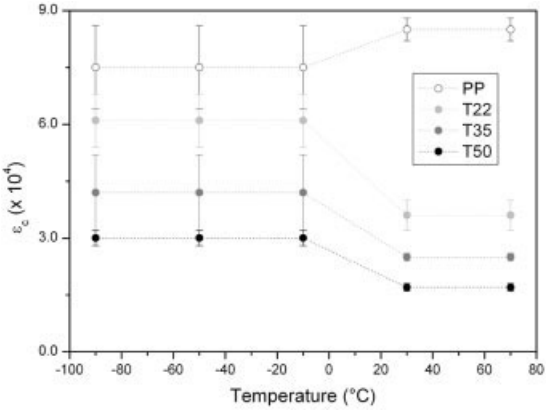

Figure 9 Variations of the dynamic critical strain ε_c as a function of the temperature for the different materials.

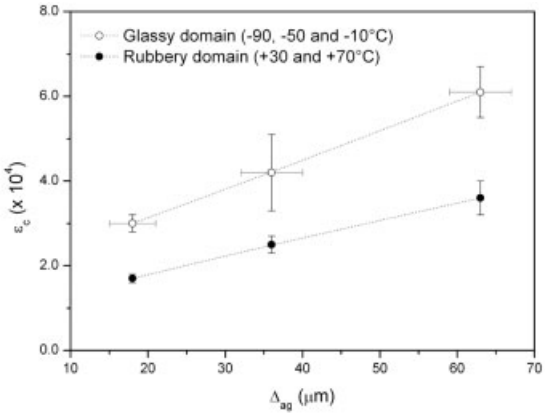

Figure 10 Variations of the dynamic critical strain ε_c as a function of the interaggregate surface-to-surface distance Δ_{ag} in the glassy and rubbery regions.

On the basis of a previous morphological analysis,[19] we tried to define the key parameters governing the initiation of damages in the commingled composites. For this, a linear evolution of ε_c versus the interaggregate surface-to-surface distance, Δ_{ag}, is plotted in Figure 10, whatever the temperature range.

The increase of the Δ_{ag} values, characteristic of a better dispersion of aggregates within the polymer matrix, leads to greater values of this critical deformation of composites. Accordingly, the initiation of damages in commingled composites, exhibiting homothetical morphology, seems to be governed by the interaggregate distance and by the molecular motions of polypropylene chains.

Influences of filler content and temperature on the failure of composites

The evolution of the failure behavior of unidirectional commingled composites is also analyzed as a function of filler content or temperature. Correlations between dynamic mechanical properties, in particular the failure strain (ε_{rupt}), and morphological parameters evaluated through 2D image processing are carried out. In addition, SEM observations of composites are done to highlight the different failure modes, i.e., adhesive or cohesive failure, as a function of temperature and filler content (Fig. 11).

Two regions can be distinguished:

- For failure strain, ε_{rupt}, higher or equal to 0.35%, a cohesive failure occurs in the rubbery domain for all the materials studied and in the glassy region for the unfilled polymer and the T22 composite. These results, in agreement with those of Gamstedt et al.,[2] show that the matrix deformation seems to play a major role in the macroscopic behavior of commingled composites. Similar frac-

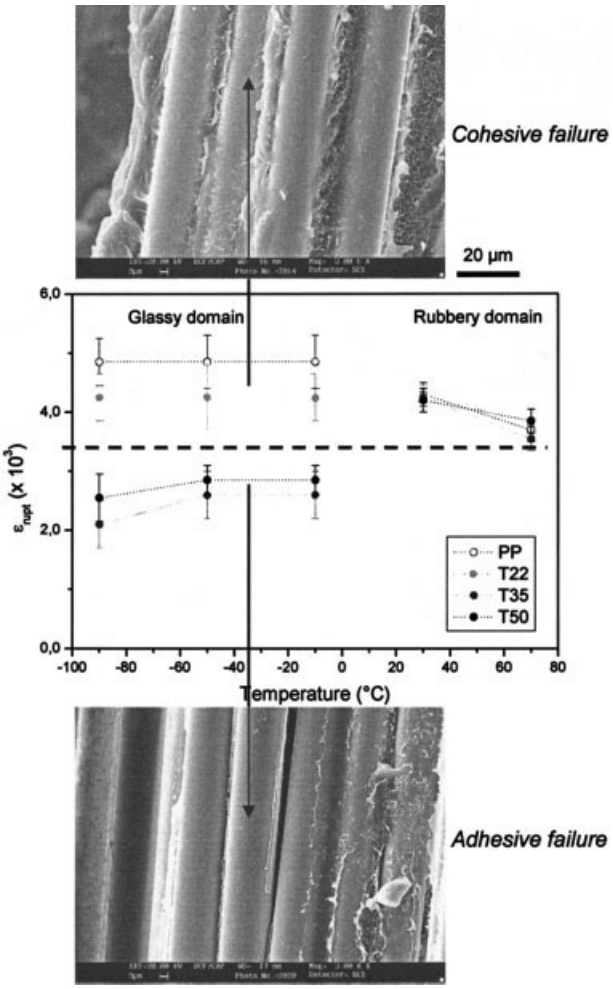

Figure 11 Variations of the dynamic failure strain ε_{rupt} versus the temperature for the different materials. Fractographic SEM observations are also shown.

tographic SEM observations have been made on the composites analyzed; i.e., debonded aggregates can be observed for the different materials (Fig. 12).

- For ε_{rupt} lower than 0.35%, an adhesive failure has been observed for the composites filled with 35 or 50% of glass fibers in the glassy state. The surface of debonded fibers appears smooth and many prints of fibers are visible in the polymer matrix. Accordingly, the interfacial debonding seems to play the principal role in the failure behavior of the highest filled materials in this temperature range.

The transition between these two failure modes can explain the decrease in the macroscopic failure strain observed for the highest filled composites. The different states of stress at the fiber–polymer interface can also be evoked to explain the differences in these values. Consequently, to reduce the transverse brittleness of commingled composites, we propose to improve the interfacial strength between aggregates and polymer by favoring, for example, the development of a "smart" interphase between fibers and polymer.

CONCLUSIONS

Several correlations between the spatial distribution of glass fibers and the mechanical behavior of commingled composites have been proposed in this work. From the morphological analysis, it has been shown that (i) fibers are packed into clusters, and (ii) aggregates are well dispersed within a modified polypropylene matrix, whatever the volume fraction of fillers. The composite is then described as a two-phase material, i.e., aggregates dispersed within the polypropylene matrix. The prediction of the viscoelastic behavior of commingled composites is then explained based on these geometrical considerations.

As a first step, the dynamic mechanical behavior of aggregates, exhibiting transversely isotropic properties, is assessed using both the Christensen and Lo's and Hashin and Rosen's models. Based on the volume fractions of the different phases, determined through a previous 2D image processing, it has been shown that the transverse Young's modulus of aggregates is greater than that of the highest filled materials in the whole temperature range.

As a second step, the dynamic mechanical behavior of unidirectional composites is assessed by using again the same models. Such an approach predicts the increase in the reinforcement effect of the polymer matrix induced by the aggregates in the glassy domain. The differences observed between experimental and simulated data of the transverse Young's modulus of composites for temperatures higher than about 0°C have then been related to global modifications in the microstructure of the polypropylene matrix induced by the fibers.

To confirm this explanation, microindentation tests were performed at 25°C. The greater values of the microhardness of polymer matrix compared with that

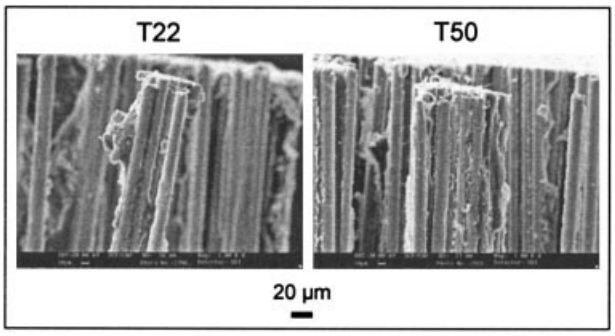

Figure 12 Fractographic SEM observations of the T22 and T50 composites.

of the unfilled polymer confirm the global modifications of the microstructure of the polypropylene matrix previously revealed by DSC analysis. These changes affect not only the molecular motions of the polypropylene chains but also the mechanical properties of composites at high temperatures.

Different origins of the transverse brittleness of unidirectional composites are proposed in the literature. To differentiate these origins, correlations between morphological parameters and macroscopic mechanical behavior of commingled composites have been made. In particular, it has been shown that the critical strain, ε_c, is a genuine probe of the initiation of damage in the composites. The increase in the values of ε_c as a function of the filler content has been related to the interaggregate surface-to-surface distance over a wide range of temperatures. Lastly, different mechanisms of failure, i.e., adhesive or cohesive failure, have been observed as a function of temperature or volume fraction of fibers. A transition between these two failure modes has then been noticed, related to the increase in the molecular motions of PP chains with increase in the temperature. In the glassy domain, the different failure modes have been detected for the different materials analyzed, whereas in the rubbery region, only a cohesive failure has been observed.

A finite-element analysis is in progress to identify the different mechanisms of damage and the failure modes observed as a function of volume fraction of fillers or temperature.

APPENDIX

The complex transverse Young's modulus of unidirectional fiber composites, E^*_T, is given by the following equation:

$$E_T^* = \frac{2}{\frac{1}{2K_T^*} + \frac{1}{2G_{TT}^*} + \frac{2\nu_{LT}^{*2}}{E_L^*}}$$

This expression required the determination of the following elastic and then viscoelastic parameters of unidirectional fiber composites: G_{TT} the transverse shear modulus, K_T the plane-strain bulk modulus, E_L the longitudinal Young's modulus, and ν_{LT} the longitudinal Poisson's ratio.

The transverse shear modulus, G_{TT}, is predicted by a (3)-phase self-consistent scheme derived from Christensen and Lo's model.[22,23] The solution for the complex transverse shear modulus, G^*_{TT}, is given by the solution of the following quadratic equation:

$$A\left[\frac{G_{TT}^*}{G_m^*}\right]^2 + B\left[\frac{G_{TT}^*}{G_m^*}\right] + C = 0$$

where subscript m refers to the matrix and constants A, B, and C are defined by the following relationships:

$$A = 3V_f(1-V_f)^2\left[\frac{G_f}{G_m} - 1\right] \times G_m \left[\frac{G_f}{G_m} + \eta_f\right] + \left[\frac{G_f}{G_m}\eta_m + \eta_f\eta_m - \left(\frac{G_f}{G_m}\eta_m - \eta_f\right)V_f^3\right] \times \left[\eta_m V_f\left(\frac{G_f}{G_m} - 1\right) - \left(\frac{G_f}{G_m}\eta_m + 1\right)\right]$$

$$B = -6V_f(1-V_f)^2\left[\frac{G_f}{G_m} - 1\right]\left[\frac{G_f}{G_m} + \eta_f\right] + \left[\frac{G_f}{G_m}\eta_m + \left(\frac{G_f}{G_m} - 1\right)V_f + 1\right] \times \left[(\eta_m - 1)\left(\frac{G_f}{G_m} + \eta_f\right) - 2V_f^3\left(\frac{G_f}{G_m}\eta_m - \eta_f\right)\right] + (\eta_m + 1)V_f\left(\frac{G_f}{G_m} - 1\right) \times \left[\frac{G_f}{G_m} + \eta_f + \left(\frac{G_f}{G_m}\eta_m - \eta_f\right)V_f^3\right]$$

$$C = 3V_f(1-V_f)^2\left[\frac{G_f}{G_m} - 1\right] \times \left[\frac{G_f}{G_m} + \eta_f\right] + \left[\frac{G_f}{G_m}\eta_m + \left(\frac{G}{G}\eta_m - 1\right)V_f + 1\right] \times \left[\frac{G_f}{G_m} + \eta_f + \left(\frac{G_f}{G_m}\eta_m - \eta_f\right)V_f^3\right]$$

with $\eta_m = 3 - 4\nu_m$ and $\eta_f = 3 - 4\nu_f$

The other mechanical parameters are derived from the composite cylinder assemblage approach proposed by Hashin and Rosen:[21]

$$K_T^* = K_m + \frac{V_f}{\frac{1}{K_f - K_m} + \frac{1 - V_f}{K_m + G_m}}$$

$$G_{LT}^* = G_m + \frac{V_f}{\frac{1}{G_f - G_m} + \frac{1 - V_f}{2G_m}}$$

$$E_L^* = E_m(1 - V_f) + E_f V_f + \frac{4(\nu_f - \nu_m)^2 V_f(1 - V_f)}{\frac{(1 - V_f)}{K_f} + \frac{V_f}{K_m} + \frac{1}{G_m}}$$

$$\nu_{LT}^* = \nu_m(1 - V_f) + \nu_f V_f + \frac{(\nu_f - \nu_m)\left(\frac{1}{K_m} - \frac{1}{K_f}\right)V_f(1 - V_f)}{\frac{(1 - V_f)}{K_f} + \frac{V_f}{K_m} + \frac{1}{G_m}}$$

with $K_i = k_i + G_i/3$ and $k_i = + E_i/3(1 - 2\nu_i)$, i = m, f

The authors acknowledge the assistance of M. Romeyer in taking the SEM images (LCME –University of Savoie).

References

1. Benzarti, K.; Cangemi, F.; Dal Maso, F. Compos A 2001, 32, 197.
2. Gamstedt, E. K.; Berglund, L. A.; Peijs, T. Compos Sci Technol 1999, 59, 759.
3. Honoré, J. C.; DEA Sci. Report; University of Savoie, Le Bourget du Lac, 2003.
4. Asp, L. E.; Berglund, L. A.; Talreja, R. Compos Sci Technol 1996, 56, 657.
5. Gao, S.-L.; Mäder, E. Compos A 2002, 33, 559.
6. Podgaiz, R. H.; Williams, R. J. J. Compos Sci Technol 1997, 57, 1071.
7. Vendramini, J.; Mélé, P.; Merle, G.; Albérola, N. D. J Appl Polym Sci 2000, 77, 2513.
8. Mäder, E.; Moos, E., Karger-Kocsis, J. Compos A 2001, 32, 631.
9. Albérola, N. D.; Merle, G.; Benzarti, K. Polymer 1999, 40, 315.
10. Vendramini, J. Ph.D. Thesis, INSA, 1999.
11. Dubouloz-Monnet, F.; Mélé, P.; Albérola, N. D. Compos Sci Technol 2005, 65, 437.
12. Dubouloz-Monnet, F.; Bas, C.; Albérola, N. D. J Macromol Sci Phys 2002, B41, 671.
13. Amitay-Sadovsky, E.; Wagner, H. D. Polymer 1998, 39, 2387.
14. Amitay-Sadovsky, E.; Wagner, H. D. J Polym Sci Part B: Polym Phys 1999, 37, 523.
15. Mc Crum, N. G. Makromol Chem 1959, 34, 50.
16. Boyd, R. H. Polymer 1985, 26, 323.
17. Reneker, D. H.; Mazur, J. J Phys C10, 1985, 46, 499.
18. Takayanagi, M. In Molecular Basis of Transition and Relaxation; Heiler, D. L., Ed.; Midland Macromolecular Monographs; Gordon and Breach Science Publishers: New York, 1978; Vol. 4, p 117.
19. Dubouloz-Monnet, F.; Mélé, P.; Albérola, N. D. J Appl Polym Sci 2005, 97, 1038.
20. Benzarti, K. Ph.D. Thesis, University Claude Bernard, 1997.
21. Hashin, Z.; Rosen, W. B. J Appl Mech 1964, 31, 223.
22. Christensen, R. M.; Lo, K. H. J Mech Phys Solids 1979, 27, 315.
23. Christensen, R. M.; Lo, K. H. J Mech Phys Solids 1986, 34, 639.
24. Dickie, R. A. J Appl Polym Sci 1973, 17, 45.
25. Agbossou, A.; Bergeret, A.; Benzarti, K.; Albérola, N. D. J Mater Sci 1993, 28,. 1963.
26. Hashin, Z. Int J Solids Struct 1970, 6, 797.
27. Hashin, Z. J Mech Phys Solids 1979, 46, 543.
28. Kharrat, M.; Chateauminois, A.; Carpentier, L.; Kapsa, P. Compos A 1997, 28, 39.
29. Zidi, M.; Carpentier, L.; Chateauminois, A.; Sidoroff, F. Compos Sci Technol 2000, 60, 429.
30. Zidi, M.; Carpentier, L.; Chateauminois, A.; Kapsa, P.; Sidoroff, F. Compos Sci Technol 2001, 61, 369.
31. Ochiai, S.; Tanaka, H.; Kimura, S.; Tanaka, M.; Hojo, M.; Okuda, K. Composites Sci Technol 2003, 63, 1027.